

# Interplay between Mach cone and radial expansion and its signal in $\gamma$ -jet events

Yasuki Tachibana\*

*Theoretical Research Division, Nishina Center, RIKEN, Wako 351-0198, Japan and  
Department of Physics, Sophia University, Tokyo 102-8554, Japan*

Tetsufumi Hirano

*Department of Physics, Sophia University, Tokyo 102-8554, Japan*

(Dated: March 6, 2022)

We study the hydrodynamic response to jet quenching in expanding quark-gluon plasma (QGP) and its signal in the resulting particle distribution. The ideal hydrodynamic simulations of the  $\gamma$ -jet events in heavy-ion collisions are performed in a full  $(3 + 1)$ -dimensional setup. The jet-induced Mach cone and the radial expansion of the background mutually push and distort each other. As a result, the particle emission is suppressed in the direction in which the radial flow is pushed back by the Mach cone when the jet path is an off-central one. This is the direct signal of hydrodynamic response to the jet and, moreover, includes information about the jet path in the expanding QGP fluid.

PACS numbers: 25.75.-q, 12.38.Mh, 25.75.Ld, 25.75.Bh

## I. INTRODUCTION

In heavy-ion collisions at the BNL Relativistic Heavy Ion Collider (RHIC) and at the CERN Large Hadron Collider (LHC), a bulk matter consisting of deconfined quarks and gluons, so-called quark-gluon plasma (QGP), is created. One of the key properties of QGP is fluid-dynamical behavior which is well described by relativistic hydrodynamics [1–9]. The fluidity implies strong coupling among the constituents of QGP. At the same time, QGP has a large stopping power against the propagation of energetic partons produced in the initial hard scatterings. These partons do not take part in the hydrodynamic bulk evolution and are subject to traverse the QGP medium because of their large transverse momenta. During the propagation, jets deposit their energies and momenta via the strong interaction with the QGP medium. This phenomenon is called jet quenching [10–16]. As a consequence of the jet quenching, jet yields in heavy-ion collisions are suppressed compared to that in proton-proton collisions where the QGP medium is not produced [17–19]. In recent heavy-ion collision experiments at LHC, the large center-of-mass energy made available detailed measurements of fully reconstructed jets with large transverse momenta  $p_{T,\text{jet}} > 100 \text{ GeV}/c$  [17–32]. The full jet evolution in the QGP has been actively studied also theoretically [33–53].

For QGP, the energetic light-quarks and gluons can be considered supersonic moving sources of the energy and momentum. Assuming that QGP responds hydrodynamically to the jet, the Mach cone, namely the conical shock wave, is excited when the deposited energy and momentum diffuse inside the medium. In early studies, motivated by the double-hump structure in the away-side of azimuthal correlations [54–57] as the signal of

the Mach cone, many theoretical studies concerning the medium response to the jet were conducted to explain it [58–69]. However, it has turned out that the double-hump structure is well reproduced by the contribution of the anisotropic flow originating from the initial geometrical fluctuation of the nucleons in the heavy ions rather than by that of the Mach cone [6, 69–72]. Recently, the hydrodynamic response to the jet quenching was focused on again because it affects various observables in detailed measurements with full jet reconstruction. The enhancement of low- $p_T$  particles away from the quenched jets [21, 31] can be interpreted as a consequence of the energy-momentum transport by the Mach cone [73]. The soft particles from the medium excitation affect also the fragmentation functions and the jet transverse profile [43, 74]. A flow flux behind the propagating parton is generated by the momentum deposition and fills in the Mach cone. The flow following the energetic partons is called the diffusion wake and can significantly modify the jet structure inside the jet cone.

As well as the formation of a Mach cone is a clear manifestation of the fluidity of QGP, its structure is characterized by key properties of QGP, e.g., sound velocity, viscosity, and stopping power. The study of this unique phenomenon involving a shock wave could provide us a great opportunity to extract the property of QGP. However, the observables in heavy-ion collisions are the particle spectra at the final state of the event and the developing Mach cone itself cannot be seen directly. Therefore, it is necessary to understand how the signal of the hydrodynamic response to the jet propagation appears in the consequent particle distribution.

In this paper, we study the hydrodynamic response to jet quenching in the QGP fluid. The background QGP fluid in heavy-ion collisions expands at relativistic flow velocity. The shape of the Mach cone is distorted by the background expansion, which affects significantly the resulting particle distribution [61, 64, 66, 68, 73, 75, 76].

---

\* yasuki.tachibana@mail.ccnu.edu.cn

It should be also noted that the Mach cone has three-dimensional structure and violates the boost invariance that the medium profile is supposed to have as an approximate symmetry around midrapidity. We describe the whole dynamics of the medium including the interplay between the response to jet quenching and the background expansion by numerically solving the  $(3+1)$ -dimensional relativistic hydrodynamic equations with source terms. We perform simulations of  $\gamma$ -jet events in central Pb-Pb collisions at the LHC energy and see how the Mach cone develops in the *expanding* medium. Then we investigate how the effect of the hydrodynamic response to jet quenching can be seen in the particle distribution after the hydrodynamic evolution. We show that the particle production is suppressed in a certain direction depending on the jet path in the medium as a result of the interplay between the Mach cone and the radial expansion. We also show that this feature can be clearly seen even in the event-averaged azimuthal angle distribution by introducing the trigger bias for the transverse momenta of the jet and the photon.

The paper is organized as follows. First, we present the formulation of the model employed in this work in Sec. II. In Sec. III, we present the results of the simulations of  $\gamma$ -jet events in the heavy-ion collisions. Section IV is devoted to summary and concluding remarks. In the following, the collision axis is taken as the  $z$ -axis and the incoming Pb nuclei collide at  $(t, z) = (0, 0)$ . We also use the Milne coordinates  $(\tau, x, y, \eta_s)$ , where  $\tau = (t^2 - z^2)^{1/2}$  is the proper time and  $\eta_s = (1/2) \ln[(t+z)/(t-z)]$  is the spacetime rapidity.

## II. METHOD OF ANALYSIS

### A. Hydrodynamic equation with source terms

Through a strong interaction with the medium, energetic partons lose their energy and momentum. We assume that the lost energy and momentum are instantaneously thermalized due to the strong interaction and are transmitted to QGP evolving as a fluid. The equation of motion of the fluid with incoming energy and momentum is given by

$$\partial_\mu T^{\mu\nu}(x) = J^\nu(x), \quad (1)$$

where  $T^{\mu\nu}$  is the energy-momentum tensor of the fluid and  $J^\nu$  is the source term which is the four-momentum density incoming from traversing partons to the fluid. Here, the medium is modeled as an ideal fluid, whose energy-momentum tensor can be decomposed as

$$T^{\mu\nu} = (\varepsilon + p) u^\mu u^\nu - p \eta^{\mu\nu}, \quad (2)$$

where  $\varepsilon$  is the energy density,  $p$  is the pressure,  $u^\mu$  is the flow four-velocity, and  $\eta^{\mu\nu} = \text{diag}(1, -1, -1, -1)$  is the Minkowski metric. Here, we employ a simple form of the

source term for a jet traversing the QGP fluid:

$$J^\mu(x) = -\frac{dp_{\text{jet}}^\mu}{dt} \delta^{(3)}(\mathbf{x} - \mathbf{x}_{\text{jet}}(t)). \quad (3)$$

We transform the hydrodynamic equations (1) to the ones in the Milne coordinate by performing the Lorentz transformation. The space-time evolution of the medium created in heavy-ion collisions is described by solving the equations in the Milne coordinate numerically. As an equation of state needed to close the system of equations, we employ the one from recent lattice QCD calculations [77]. Because Eq. (1) can describe both the hydrodynamic response to jet propagation and the expansion of the QGP, the interplay between them is automatically included in this framework.

### B. Energy loss

We model partons traveling through QGP as massless particles and neglect their structure. The jet particles move at the speed of light and deposit their energy and momentum via the strong interaction with the medium. We use the jet energy-loss of the form [68],

$$\frac{dp_a^0}{dt} = -\left[\frac{T(t, \mathbf{x}_a(t))}{T_0}\right]^3 \frac{dE}{dl}\bigg|_0, \quad (4)$$

where  $T_0$  is the reference temperature and  $dE/dl|_0$  is the energy-loss rate at  $T_0$ . In this study, the jet trajectories are restricted to be straight in the transverse plane. The jets lose their energy when the jet particles penetrate the QGP medium with the local temperature above 160 MeV. Here we set  $T_0 = 500$  MeV and  $dE/dl|_0 = 15$  GeV/fm, which reproduces the typical values of the nuclear modification factor for jets around  $p_{T, \text{jet}} \sim 100$  GeV/ $c$  in heavy-ion collisions at LHC [17].

### C. Initial profile of the medium

A hydrodynamic description is applied to the space-time evolution of the medium after the thermalization  $\tau \geq \tau_0$ . We set the initial condition for the entropy density profile of the medium at  $\tau_0 = 0.6$  fm/ $c$  as

$$s(\tau_0, \mathbf{r}_\perp, \eta_s) = s_T(\mathbf{r}_\perp) H(\eta_s) \theta(Y_{\text{beam}} - |\eta_s|). \quad (5)$$

Here,  $Y_{\text{beam}}$  is the beam rapidity of incoming nuclei, and  $H$  represents the profile in the  $\eta_s$  direction.  $s_T$  is the transverse profile of the initial entropy density at midrapidity,

$$s_T(\mathbf{r}_\perp) = \frac{C}{\tau_0} \left[ \frac{(1-\alpha)}{2} n_{\text{part}}(\mathbf{r}_\perp) + \alpha n_{\text{coll}}(\mathbf{r}_\perp) \right], \quad (6)$$

where  $n_{\text{coll}}$  and  $n_{\text{part}}$  are the number density of nucleon-nucleon binary collisions and of participating nucleons calculated from the optical Glauber model, respectively.

For Pb-Pb collision at LHC, the parameters  $C = 19.8$  and  $\alpha = 0.14$  are fitted to reproduce the centrality dependence of multiplicity measured by the ALICE Collaboration [78, 79].

The initial profile around the midrapidity region is flat in the  $\eta_s$  direction, like the Bjorken scaling solution [80]. The flat region is smoothly connected to a vacuum at both ends by using half Gaussians:

$$H(\eta_s) = \exp \left[ -\frac{(|\eta_s| - \eta_{\text{flat}}/2)^2}{2\sigma_\eta^2} \theta \left( |\eta_s| - \frac{\eta_{\text{flat}}}{2} \right) \right], \quad (7)$$

where the parameters  $\eta_{\text{flat}} = 3.8$  and  $\sigma_\eta = 3.2$  are chosen to give the pseudorapidity distribution similar to the one obtained from the Monte Carlo Kharzeev-Levin-Nardi model for central Pb-Pb collisions [81]. It is assumed that there is no transverse flow at  $\tau = \tau_0$  and the radial expansion of the medium is driven solely by the initial pressure gradient in the transverse direction. For the initial condition of the flow velocity in the longitudinal direction, the space-time rapidity component is set to zero:  $u^{\eta_s}(\tau = \tau_0) = 0$  [80]. These initial conditions for the flow are commonly used in hydrodynamic models for heavy-ion collisions. In this study, we neglect the effect of the initial geometrical fluctuation of the nucleons in colliding nuclei and employ the smooth averaged profile. The flow driven by the initial fluctuation can modify the development of the Mach cone in the medium, which will be considered in upcoming work.

#### D. Freeze-out

To obtain the particle spectrum, we switch from the hydrodynamic description to a phase-space distribution of individual particles via the Cooper-Frye formula [82],

$$\frac{dN}{p_T dp_T d\phi_p d\eta} = \sum_i \frac{d_i}{(2\pi)^3} \int_\Sigma \frac{p^\mu d\sigma_\mu(x)}{\exp[p^\mu u_\mu(x)/T(x)] \mp_{\text{BF}} 1} \quad (8)$$

Here,  $p_T$  is the transverse momentum,  $\phi_p$  is the azimuthal angle,  $\eta$  is the rapidity, and  $\Sigma$  is the freeze-out hypersurface which is determined by assuming the isothermal freeze-out at the freeze-out temperature  $T_f$ .  $d_i$  is the degeneracy and  $\mp_{\text{BF}}$  corresponds to Bose or Fermi statistics for particle species  $i$ . We set  $T_f = 145$  MeV, which is the typical value to obtain the observed  $p_T$  spectra and not crucial for results presented here. In this study, we calculate the distribution of charged pions directly emitted from the freeze-out hypersurface and investigate how the effect of jet-induced flow appears in it. The charged pions from decays of hadron resonances after the hydrodynamic evolution are not included here. For more quantitative analysis, their contribution should be considered and are left as a subject for future study. Since the azimuthal angle distributions of the hadron resonances are expected to be similar to that of the charged pions just after the hydrodynamic evolution, the contribution from the decays can increase the amplitude of the resulting distribution.

### III. SIMULATIONS AND RESULTS

We perform simulations of the events in which one jet particle travels through the QGP medium. These correspond to  $\gamma$ -jet events originating from the pair production of one photon and one parton at initial hard scatterings. At leading order, the photon and the parton having the same initial energies propagate in opposite directions. While the parton deposits its energy and momentum, the photon freely penetrates the medium.

Actually, the energies of the observed jet and photon are not exactly the same even in proton-proton collisions due to higher order contributions. The momentum fraction of a photon tagged jet,  $x_T = p_{T,\text{jet}}/p_{T,\gamma}$ , is distributed with a finite width around a peak at  $x_T = 1$ . In  $\gamma$ -jet events in heavy-ion collisions, the energy loss of jets is observed as a shift of the peak to less than unity [24]. In this study, we neglect such higher order contributions and set the initial energies of the parton and photon to be the same in each event. The parton is regarded as a jet and travels through the medium. Furthermore, we also do not consider the structure of the jet. In reality, however, jets in heavy-ion collisions radiate gluons due to both their high virtuality (vacuum cascade) and inelastic collisions with the medium constituents (in-medium cascade). The jets have shower structures evolving during their propagation. It should be noted that, in particular, the spatial profile of jet energy deposition can affect the pattern of the medium response. In the case where the radiated gluons are emitted at small angles, the jet has a collimated structure and induces a Mach cone similar to the one in the case of one parton [83–85]. However, when the radiated gluons are emitted at large angles with sufficiently large momenta, the jet has a widespread structure and each radiated gluon becomes a separate source of a Mach cone. As a result, the medium response to the jet becomes a superposition of the distinct Mach cones and the clear conical structure cannot be seen [85]. In this study, we assume that the gluons having sufficiently large momenta are radiated only at small angle and regard them as a part of the structureless jet. To perform more realistic simulations, the inclusion of the proper  $x_T$  distribution and the jet structure evolution is necessary (as in Ref. [44]). Here we postpone it as a future study.

The shape of the medium response to the jet is also affected by the viscosity of the QGP fluid. As the shear viscosity increases, it tends to smear out the Mach cone structure because the diffusion wake is transported perpendicular to the jet and destroys the conical wave front [76, 86–88]. Nevertheless, the rather clear Mach cone structure appears in the calculation with the small shear viscosity which the QGP is expected to have. Here we neglect the small shear viscosity of the QGP and model the QGP as the ideal fluid. In this sense, the Mach cone develops with the most clear conical structure and its maximum signal is exhibited in our results.

In the simulations, we consider the completely central Pb-Pb collisions (impact parameter  $b = 0$  fm). The pro-

file of the created medium at  $\tau_0$  is isotropic in the transverse plane and the origin  $(x, y, \eta_s) = (0 \text{ fm}, 0 \text{ fm}, 0)$  is set at its center. The jet parton is supposed to be created in the transverse plane  $\eta_s = 0$  at  $\tau = 0$  and travel freely without any interaction until  $\tau_0 = 0.6 \text{ fm}/c$ . Then it starts to interact with the QGP at the same time as the beginning of the hydrodynamic bulk evolution. The space-time evolution of the medium with the incoming energy via the jet energy loss is assumed to obey Eq. (1). Without a loss of generality, we set the direction of the photon propagation as the positive  $x$  direction ( $\phi_p = 0, \eta = 0$ ) and the direction of the jet propagation as the negative  $x$  direction ( $\phi_p = \pi, \eta = 0$ ). In the completely central collisions, any path of the jets in the QGP is covered by changing only the jet production point due to rotational symmetry in the transverse plane.

### A. Energy density distribution of the medium

Figure 1 shows the energy density distributions of the medium fluid in the transverse plane at  $\eta_s = 0$  at  $\tau = 12.0 \text{ fm}/c$  for various production points for energetic partons. We can see relatively higher energy density regions which have U-shaped or V-shaped structures in Fig. 1 except for Fig. 1 (g). These are the remnants of Mach cones. The Mach cones are induced by the energy momentum deposition from jets and distorted by the radial flow in various ways depending on where they develop in the medium. In the case where the jet is produced on the negative  $x$  side and escapes from the radial flow, the radial flow pushes the wave front of the Mach cone mainly from the inside. Consequently, the shape of the Mach cone becomes rounded [Figs. 1 (a), (b), (d), and (e)]. In the case where the energetic parton travels through the off-central path in the medium, the Mach cone is drifted by the radial flow of the background and inclined to the inside of the medium. Furthermore, the Mach cone and the radial flow push each other, and thereby the Mach cone is asymmetrically distorted [Figs. 1 (f), (h), and (i)]. In an event where the jet is produced at the edge of the medium and then travels outward, the Mach cone is almost not formed [Fig. 1 (g)]. This is because the jet escapes from the hot region of the medium before the Mach cone develops.

### B. Azimuthal angle distribution

The main motivation in this paper is to study how the hydrodynamic response to jet propagation appears in the resulting particle spectra. We calculate the azimuthal angle distribution of charged pions emitted from the medium. Here, the distribution in the case without jet propagation is subtracted as a background:

$$\Delta \frac{dN_{\pi^\pm}}{d\phi_p d\eta} = \frac{dN_{\pi^\pm}}{d\phi_p d\eta} - \frac{dN_{\pi^\pm}}{d\phi_p d\eta} \Big|_{\text{no jet}}. \quad (9)$$

In this study, we focus only on the low momentum particles originating from the bulk medium and do not include the particles from jet fragmentation in the calculations. When we take an event average, each event is weighted by the jet production rate as a function of the jet creation point and initial jet transverse momentum. As the weight for the spatial distribution of the jet production points in the transverse plane, we use the number density of the binary collisions between the nucleons in a Pb-Pb collision calculated from the Glauber model. As the momentum dependence of the jet production rate, we use a power function:

$$\frac{d^2\sigma}{dp_{T,\text{jet}} dy} = \frac{1}{p_0} \left( \frac{p_0}{p_{T,\text{jet}}} \right)^\alpha, \quad (10)$$

where  $p_0 = 205 \text{ GeV}/c$  and  $\alpha = 6.43$  are parameters chosen to fit the data from the ATLAS Collaboration in  $p$ - $p$  collisions at  $\sqrt{s_{NN}} = 2.76 \text{ TeV}$  [17].

The solid line in Fig. 2 shows the azimuthal angle distribution at midrapidity after taking the event average. In this analysis, only the contribution of the charged pions with the transverse momenta between 1 and 2  $\text{GeV}/c$  is taken into account. This  $p_T$  range is employed to measure the low- $p_T$  particles associated with large- $p_T$  jets in experiments by the CMS Collaboration [32]. The average is taken over the events to the jet transverse momentum  $p_{T,\text{jet}} \geq 80 \text{ GeV}/c$  in the final state. We can see only a peak in the jet direction  $\phi_p = \pi/2$ , and the opposite side around  $\phi_p = 0$  is almost flat. Intuitively, Mach cones are expected to produce a double-hump structure around the jet direction in the azimuthal distribution by an analogy to a ring image of the Cherenkov radiation. However, such a structure cannot be obtained from this hydrodynamic calculation. We have some reasons for the absence of the double-hump structure. First, the momentum deposition of the jet induces the diffusion wake which produces a prominent peak in the spectra in the direction of jets. Second, when calculating the spectra through the Cooper-Frye formula (8), the thermal equilibrium distribution boosted by the flow velocity is used. The flow velocity distribution is not directly reflected and is smeared out in the consequent spectra. Third, since the Mach cones are largely distorted by the expansion of the medium, the Mach cones no longer have the clear conical shock front. Actually, the double-hump structure caused by the Mach cone does not exist in the observation by the CMS Collaboration [32]. In this result, any clear signal reflecting the characteristic structure of a Mach cone cannot be seen.

The dashed line and the dotted line in Fig. 2 show the results averaged over events where the jet production points are restricted in the region  $y \leq 0$  and in the region  $y \geq 0$ , respectively. These are symmetric with respect to  $\phi = 0$  and  $\pi$  due to the symmetry of the geometry across the  $z$ - $x$  plane. The average of them is equal to the result averaged over the full events. The peaks are shifted to the direction of the radial expansion and, furthermore, dips can be seen in specific directions almost perpendicular

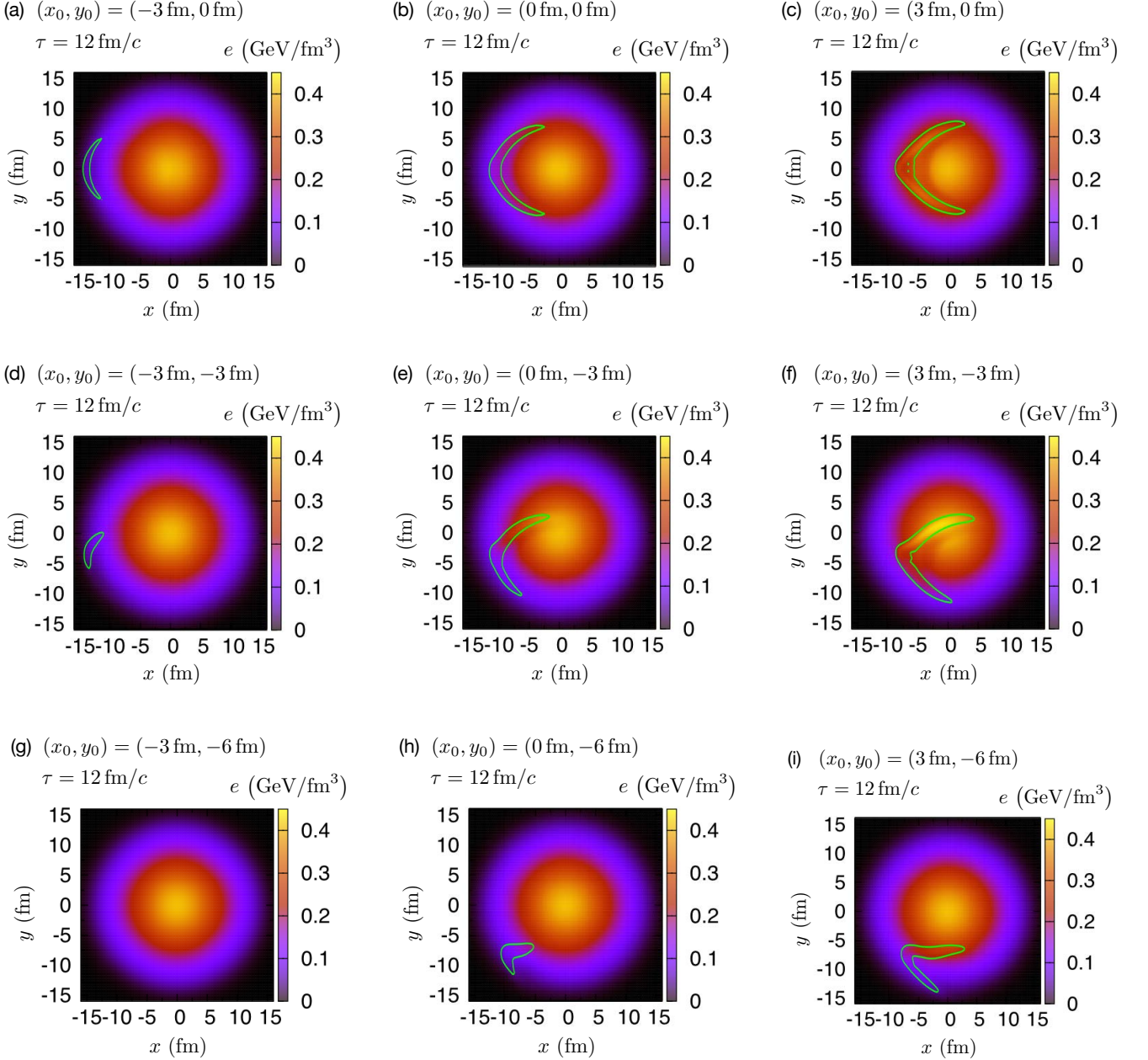


FIG. 1. (Color online) Energy density distribution of the medium fluid in the transverse plane at midrapidity  $\eta_s = 0$  for different jet production points. The snapshots are taken at  $\tau = 12.0$  fm/c. The solid lines show the higher energy density region compared to the case without jet propagation.

ular to the peaks. The appearance of such structures in the azimuthal angle distribution reflects the geometrical relation between the jet production point and the medium.

To interpret these structures, let us consider specific events. Figures 3-5 show the azimuthal angle distributions for a single event with a specific jet production point. Figure 3 shows the results in the case where the

jet production point is located in the fourth quadrant ( $x_0 = 3$  fm,  $y_0 = 0, -3, -6$  fm). We can see that the peak in the jet direction shifts to larger  $\phi$  as the distance between the jet production point and the  $x$  axis increases. This is because the fast flow of the diffusion wake is pushed and bent by the radial flow of the background medium. At the edge of the medium, the radial flow becomes faster and pushes the diffusion wake strongly.

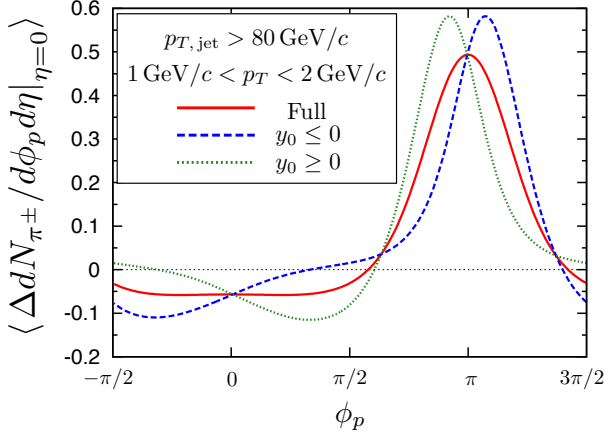


FIG. 2. (Color online) Event-averaged azimuthal angle distributions of charged pions with  $1 < p_T < 2 \text{ GeV}/c$  subtracted by the background. The trigger threshold for the jet transverse momentum at final state is  $p_{T,\text{jet}} > 80 \text{ GeV}/c$ . The solid line is the result averaged over all the triggered events. The dashed line and the dotted line are the results averaged over events with the jet production points in the region  $y \le 0$  and in the region  $y \ge 0$ , respectively.

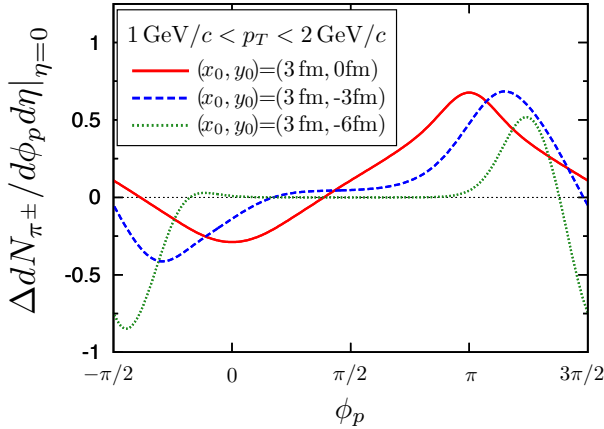


FIG. 3. (Color online) Azimuthal angle distributions of charged pions with  $1 < p_T < 2 \text{ GeV}/c$  subtracted by the background. The solid line, the dashed line, and the dotted line are the results for the events with the jet production point at  $(x_0, y_0) = (3.0 \text{ fm}, 0 \text{ fm})$ ,  $(3.0 \text{ fm}, -3.0 \text{ fm})$ , and  $(3.0 \text{ fm}, -6.0 \text{ fm})$ , respectively.

When the jet is produced at  $(x_0, y_0) = (3 \text{ fm}, 0 \text{ fm})$ , the number of low  $p_T$  particles in the direction opposite to the jet ( $\gamma$  direction) decreases. While the jet travels toward the center of the medium, the Mach cone propagates squarely against the radial flow. As a result, the particle emission in the  $\gamma$  direction is suppressed. In Fig. 3, one can see a dip at  $\phi_p \sim -\pi/4$  in the case of the jet produced at  $(x_0, y_0) = (3 \text{ fm}, -3 \text{ fm})$  and at  $\phi_p \sim -\pi/2$

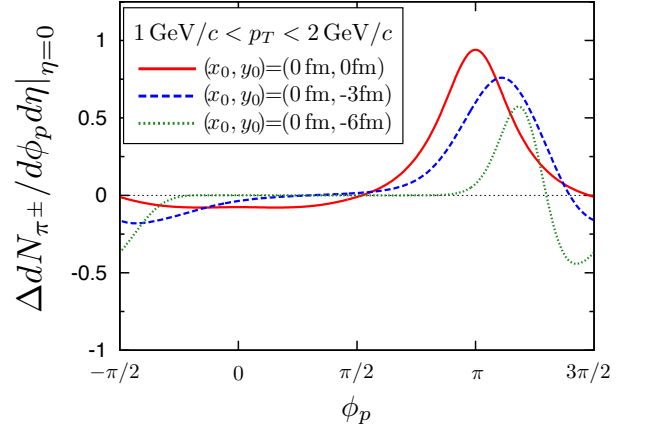


FIG. 4. (Color online) Azimuthal angle distributions of charged pions with  $1 < p_T < 2 \text{ GeV}/c$  subtracted by the background. The solid line, the dashed line, and the dotted line are the results for the events with the jet production point at  $(x_0, y_0) = (0 \text{ fm}, 0 \text{ fm})$ ,  $(0 \text{ fm}, -3.0 \text{ fm})$ , and  $(0 \text{ fm}, -6.0 \text{ fm})$ , respectively.

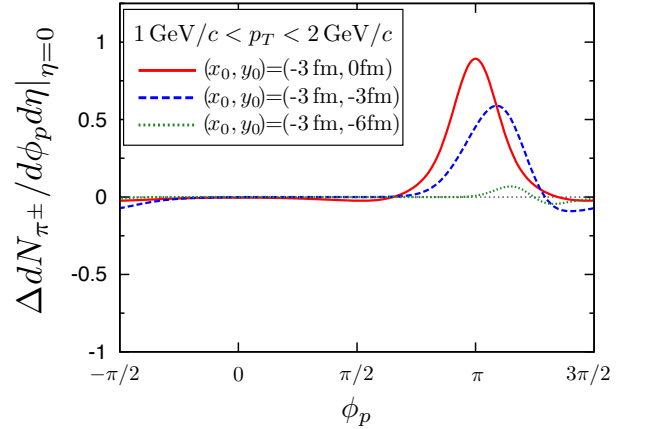


FIG. 5. (Color online) Azimuthal angle distributions of charged pions with  $1 < p_T < 2 \text{ GeV}/c$  subtracted by the background. The solid line, the dashed line, and the dotted line are the results for the events with the jet production point at  $(x_0, y_0) = (-3.0 \text{ fm}, 0 \text{ fm})$ ,  $(-3.0 \text{ fm}, -3.0 \text{ fm})$ , and  $(-3.0 \text{ fm}, -6.0 \text{ fm})$ , respectively.

in the case of  $(x_0, y_0) = (3 \text{ fm}, -6 \text{ fm})$ .

Figure 6 is an illustration of how this dip appears in a certain direction in the azimuthal angle distribution. When the jet path is away from the center of the medium, the induced Mach cone violates the symmetry of the flow profile with respect to the  $x$  axis (V-shaped region in Fig. 6). In particular, the wave front of the Mach cone on the center side of the medium develops more largely than that on the outer side because of the higher temperature and pushes back the radial flow strongly in a certain

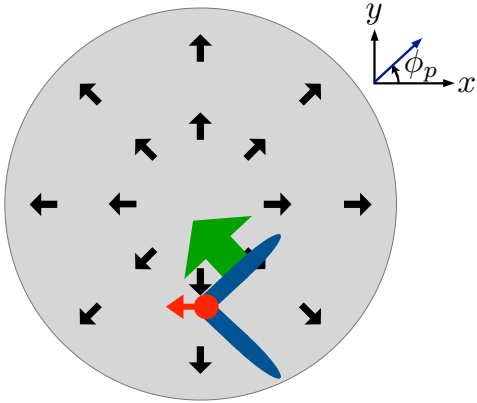


FIG. 6. (Color online) Schematic picture of the transverse plane  $\eta_s = 0$  to illustrate how the Mach cone propagating in the expanding QGP suppresses the particles in a certain direction. The radial flow is induced by the expansion of the background QGP medium (arrows pointing in the radial direction). The jet (small circle with a small arrow at the top of the V-shaped region) travels through the lower half region of the QGP and induces the Mach cone (V-shaped region). During propagation, the wave front of the Mach cone pushes back the radial flow (large arrow from the side of the V-shaped region). As a result, the particles emitted in the direction opposite to the large arrow are suppressed.

direction (large arrow from the side of the V-shaped region in Fig. 6). Thereby, in the direction in which the radial flow is held back by the wave front on the center side, the particle emission is suppressed.

Figure 4 shows the results when the jet production point is set on the negative  $y$  axis ( $x_0 = 0 \text{ fm}, y_0 = 0, -3, -6 \text{ fm}$ ). The shifts of the peaks in the jet direction and the dips can also be seen. The angle between the dip direction and the  $\gamma$  direction is large compared to the ones in the case of the jet production point in the fourth quadrant. This is because the direction of the radial flow pushed back by the Mach cone is shifted to the clockwise direction depending on the jet path in the medium. In Fig. 5, the results in the case of the jet produced in the third quadrant ( $x_0 = -3 \text{ fm}, y_0 = 0, -3, -6 \text{ fm}$ ) are shown. The structures in the  $\gamma$  direction are almost flat. In these cases, the jet propagates away from the radial flow. The induced Mach cone is pushed mainly from the inside by the radial flow in the jet direction and does not affect the radial flow in the  $\gamma$  direction.

As mentioned above, the interplay between Mach cone and radial expansion appears as a dip in azimuthal distributions. It can be referred to as the signal of the Mach cone and its direction and depth vary with the jet path in the expanding QGP medium. The trigger threshold for jets can constrain the jet production point [44, 89–91]. Jets with lower energies are produced much more frequently because the production rate is a steeply decreasing function of the jet energy. However, when jets

TABLE I. Ratios of the number of events with triggers for both photon ( $110 < p_{T,\gamma} < 120 \text{ GeV}/c$ ) and jet momenta shown in Figs. 8 (a)-(d) to that (middle column) with the triggers for both photon ( $110 < p_{T,\gamma} < 120 \text{ GeV}/c$ ) and jet ( $p_{T,\text{jet}} > 80 \text{ GeV}/c$ ) and that (right column) with the trigger only for the jet ( $p_{T,\text{jet}} > 80 \text{ GeV}/c$ ) as shown in Fig. 7.

$p_T$ range for jet trigger (GeV/c)	With $\gamma$ trigger	Without $\gamma$ trigger
$110 < p_{T,\text{jet}} < 120$	0.06	0.012
$100 < p_{T,\text{jet}} < 110$	0.26	0.047
$90 < p_{T,\text{jet}} < 100$	0.47	0.085
$80 < p_{T,\text{jet}} < 90$	0.21	0.037

travel through the center of the medium, jets with low initial energy are hardly triggered in the final state because of the large energy loss. Therefore, if the trigger is set to choose small-energy-loss events, the distribution of the jet production point in the triggered events is biased to the surface of the medium. We here show how the distribution of the jet production point and the resulting azimuthal angle distribution of the soft particles are varied depending on the trigger threshold.

Figure 7 shows the distribution of the jet production point when the trigger threshold for the jet transverse momentum in the final state is set to  $p_{T,\text{jet}} > 80 \text{ GeV}/c$ . The jet particles are produced likely near the central region because the number of binary collisions between the nucleons is a maximum at the center and goes to zero at the edge of the reaction region. However, we can see that the events in which the jet is produced near the surface of the medium and then escapes to the outside are dominant. This is because the lower energy jets which are produced more frequently can survive with enough transverse momenta to be triggered in such events.

Next, we introduce trigger thresholds for the transverse momentum of the jet both in the final state and in the initial state. We can regard the initial transverse momentum of the jet as the transverse momentum of the photon  $p_{T,\gamma}$  in a  $\gamma$ -jet event. Here, the trigger of the photon is fixed so that its transverse momentum is  $100\text{--}120 \text{ GeV}/c$ . Figure 8 shows the distribution of the jet production point for different  $p_{T,\text{jet}}$  ranges of the trigger. When the trigger is set to extract small energy loss events, the detected jets are created in the crescent-shaped region near the surface of the medium [Figs. 8 (a) and (b)]. However, when large-energy-loss events are extracted by the trigger, the detected jets are created in the region near the center in which the path length in the medium is to be long [Figs. 8 (c) and (d)]. Ratios of the number of these events to that when the jet trigger is set to  $p_{T,\text{jet}} > 80 \text{ GeV}/c$  are shown in Table I. The middle column is the ratio to the number of events when the trigger also for photon transverse momentum is set to  $110\text{--}120 \text{ GeV}/c$ . The sum of these ratios is equal to unity. The right-hand column is the ratio to that without the trigger for the photon which corresponds to the jet production point distribution shown in Fig. 7.



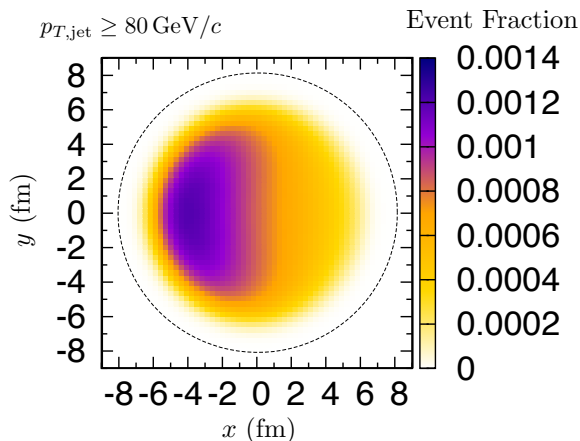


FIG. 7. (Color online) Distribution of the jet production point for the  $\gamma$ -jet events when the trigger threshold for the jet transverse momentum in the final state is set to  $80 \text{ GeV}/c$ .

Shown in Fig. 9 are the event-averaged azimuthal angle distributions at midrapidity when the  $p_{T,\text{jet}}$  trigger is  $100\text{--}110 \text{ GeV}/c$  and  $110\text{--}120 \text{ GeV}/c$ . The trigger for  $p_{T,\gamma}$  is also set to  $110\text{--}120 \text{ GeV}/c$ . Two dips can be seen at both ends of the peak in the jet direction. This structure reflects the development of the Mach cone in the expanding medium and the crescent shape of the jet production point distribution. When a jet parton is produced at the edge of the crescent, the wave front of the Mach cone on the center side pushes back the radial flow significantly. The resulting spectrum for such an event has a dip in the direction in which the jet path lies. The dips around  $\phi = \pi/2$  are due to the contribution of the events with a jet created in  $y \geq 0$  and the dips around  $\phi = 3\pi/2$  are due to the contribution of the events with a jet created in  $y \leq 0$ . When a jet is created at the center of the crescent, the Mach cone is pushed mainly from the inside by the radial flow. In such an event, the spectrum is almost flat except for the peak in the jet direction as shown by the solid line in Fig. 5. Therefore, the dips are not smeared out by the contribution of such events and can be clearly seen even after taking the event average owing to the trigger bias. Figure 10 shows the event-averaged azimuthal angle distributions at midrapidity when the  $p_{T,\text{jet}}$  triggers are  $90\text{--}100 \text{ GeV}/c$  and  $80\text{--}90 \text{ GeV}/c$ . In these  $p_{T,\text{jet}}$  ranges of the jet trigger, the dips at both ends of the peaks cannot be seen. As seen in Fig. 8 (c) and (d), the distribution of the jet production point is concentrated so that the jets take long paths through the central region of the QGP medium. Thus, the contribution of the events whose resulting spectra are similar to the solid line in Figs. 3 and 4 becomes dominant and the azimuthal angle distributions have simple structures.

In this analysis, we set the initial energy of the jet and the photon to be the same. The events were divided according to the jet production point by introducing trigger thresholds both for the jet and for the photon. If one

generates the photon-jet pair with a realistic  $x_T$  distribution, one can also use the  $x_T$  to control the jet production point because events with large  $x_T$  close to unity are dominated by events with small energy loss. Indeed, the distribution for small-energy-loss events [Figs. 8 (a) and (b)] are similar to the one for large- $x_T$  events of the event-by-event calculations in Ref. [44].

#### IV. SUMMARY

In this paper, we studied the hydrodynamic response of QGP to the energy-momentum deposition from jets. We formulated the model including the ideal hydrodynamic equations to describe the space-time evolution of the medium. To consider the contribution of the incoming energy and momentum from jets, the source terms were introduced to the hydrodynamic equations. In this process, we assumed that the deposited energy and momentum are instantaneously thermalized in the QGP fluid.

We performed simulations of  $\gamma$ -jet events in central Pb-Pb collisions at LHC. A massless jet particle travels through the expanding QGP fluid while depositing its energy and momentum into the fluid. Since the jet moves faster than the sound velocity of the medium, the Mach cone is induced as a hydrodynamic response to the jet propagation. The shape of the Mach cone is distorted by the background expansion and this affects significantly the resulting particle distribution. Especially when the jet path is off central in the medium, the distortion is manifestly asymmetric.

Then how the hydrodynamic response to the jet quenching can be reflected in the resulting particle spectra in heavy-ion collisions was studied. We calculated the event-averaged azimuthal angle distribution of charged pions emitted from the medium after the hydrodynamic evolution. When the trigger threshold is set only for the transverse momentum of the jet in the final state, only a peak can be seen in the direction of the jet. However, when the jet production point is restricted in the upper half plane or in the lower half plane in the transverse plane, there is a dip on the side on which the jet path lies in the medium. The dip can also be seen in the azimuthal angle distribution for a single event when the jet path is away from the center of the medium. The wave front of the Mach cone holds back the radial flow and reduces the particle emission in the corresponding direction. The dip appears as a consequence of the interplay between the Mach cone and the radial expansion.

We also studied the case where trigger thresholds are set both for the jet and for the photon. The dip appears according to the jet path in the medium. The path can be restricted by setting the trigger threshold to extract the events with a specific amount of the energy loss. When the trigger threshold is set to extract small energy-loss events, two dips can be seen at both ends of the peak in the jet direction. The origin of the dips is the same



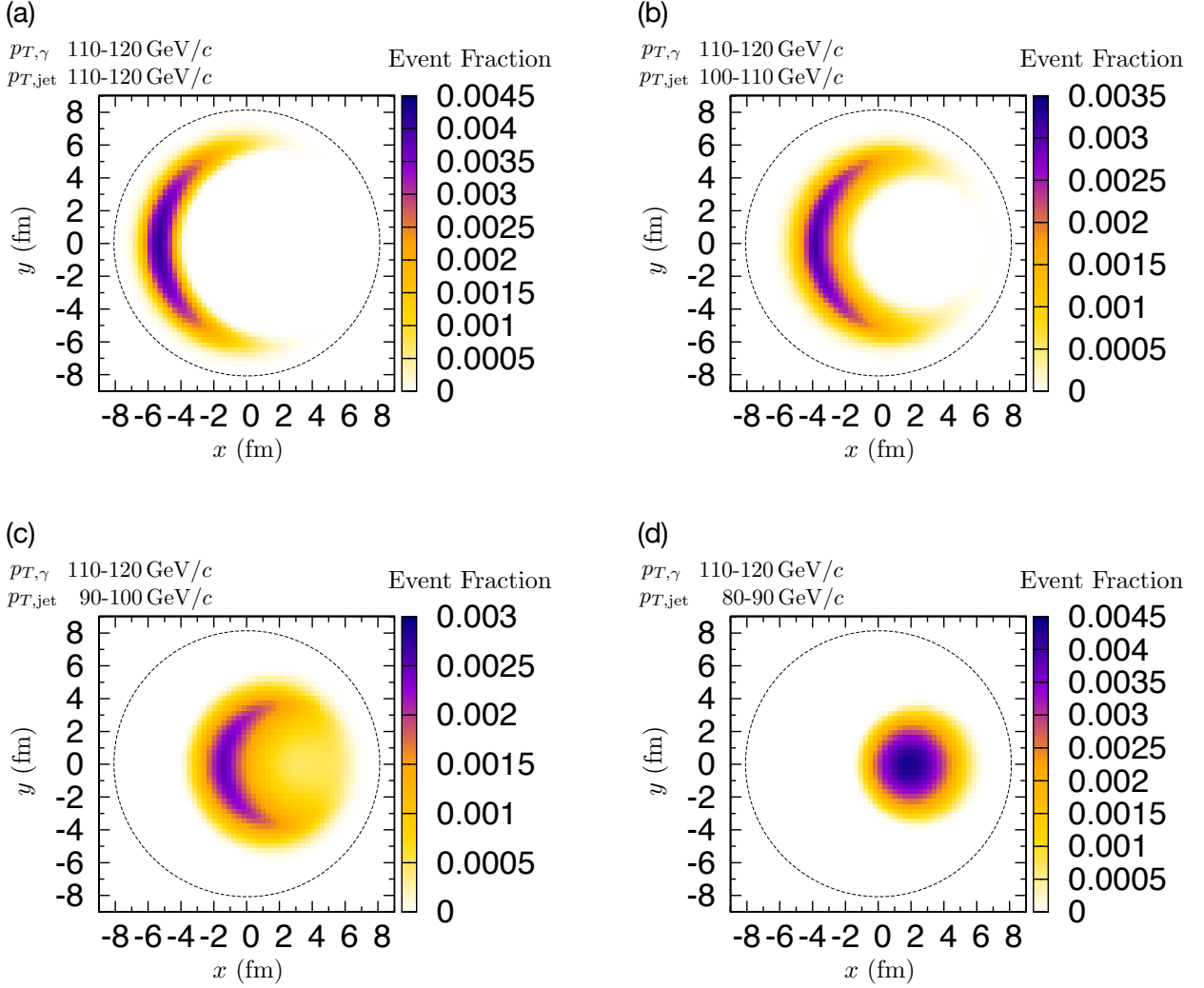


FIG. 8. (Color online) Distribution of the jet production point for different transverse momentum ranges of the jet trigger. The trigger range of the photon transverse momentum is 110-120 GeV/c. The trigger ranges of the jet transverse momentum are (a) 110-120 GeV/c, (b) 100-110 GeV/c, (c) 90-100 GeV/c, and (d) 80-90 GeV/c.

as the previous one in a single event where the jet path is away from the center. These are the consequences of the interplay between the Mach cone and the radial expansion. When large energy-loss events are extracted, the dips cannot be seen because the contribution of the events that make the dips becomes less dominant.

The dips in the azimuthal angle distribution of soft particles in  $\gamma$ -jet events can be direct signals of hydrodynamic response to jet quenching and also include the information of the jet path in the medium: which side in the transverse plane the jet path lies on and how long the jets travel through the QGP. The geometry and the radial flow of the medium play important roles in the formation of the dips and are determined by the initial

condition of the medium profile. In this work, we employed the smooth initial profile calculated from the optical Glauber model and only considered the case of impact parameter  $b = 0$ . In this case, the anisotropic flow is driven only by jet propagation. However, the fluctuation of the initial condition can always cause the anisotropy and affect the geometry and radial flow. We would like to defer the event-by-event studies including the initial fluctuation effect as a future work.

## ACKNOWLEDGMENTS

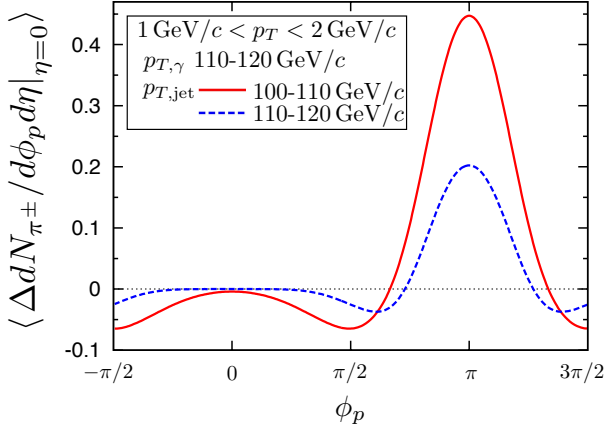


FIG. 9. (Color online) Azimuthal angle distributions of charged pions with  $1 < p_T < 2$  GeV/c subtracted by the background. The trigger range of the photon transverse momentum is 110-120 GeV/c. The trigger ranges for jet transverse momentum at final state are 100-110 GeV/c (solid line) and 110-120 GeV/c (dashed line)

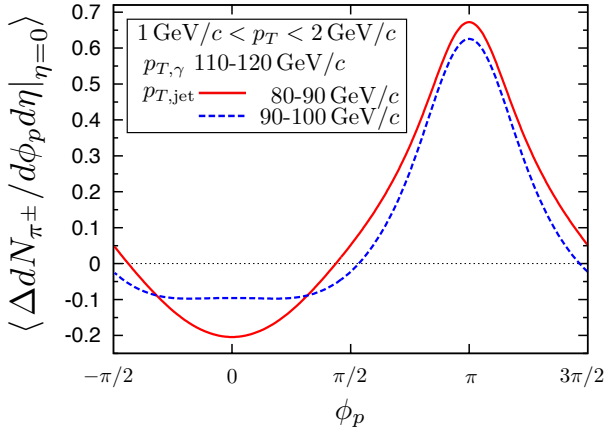


FIG. 10. (Color online) Azimuthal angle distributions of charged pions with  $1 < p_T < 2$  GeV/c subtracted by the background. The trigger range of the photon transverse momentum is 110-120 GeV/c. The trigger ranges for jet transverse momentum at final state are 80-90 GeV/c (solid line) and 90-100 GeV/c (dashed line).

The authors are grateful to G.-Y. Qin and X.-N. Wang for useful comments. The authors would also like to thank Y. Hirono for helpful discussions regarding numerical implementations. Y. T. was supported by a JSPS Research Fellowship for Young Scientists and by an Advanced Leading Graduate Course for Photon Science grant. The work was supported by JSPS KAKENHI Grants No. 13J02554 (Y. T.) and No. 5400269 (T. H.).

[1] U. W. Heinz and P. F. Kolb, Nucl.Phys. **A702**, 269 (2002), arXiv:hep-ph/0111075 [hep-ph].  
 [2] T. D. Lee, Nucl.Phys. **A750**, 1 (2005).  
 [3] M. Gyulassy and L. McLerran, Nucl.Phys. **A750**, 30 (2005), arXiv:nucl-th/0405013 [nucl-th].  
 [4] E. V. Shuryak, Nucl.Phys. **A750**, 64 (2005), arXiv:hep-ph/0405066 [hep-ph].  
 [5] T. Hirano and M. Gyulassy, Nucl.Phys. **A769**, 71 (2006), arXiv:nucl-th/0506049 [nucl-th].

[6] B. Schenke, S. Jeon, and C. Gale, Phys. Rev. Lett. **106**, 042301 (2011), arXiv:1009.3244 [hep-ph].  
 [7] Z. Qiu and U. W. Heinz, Phys. Rev. **C84**, 024911 (2011), arXiv:1104.0650 [nucl-th].  
 [8] Z. Qiu, C. Shen, and U. Heinz, Phys. Lett. **B707**, 151 (2012), arXiv:1110.3033 [nucl-th].  
 [9] C. Gale, S. Jeon, B. Schenke, P. Tribedy, and R. Venugopalan, Phys.Rev.Lett. **110**, 012302 (2013), arXiv:1209.6330 [nucl-th].

- [10] J. D. Bjorken, Fermilab, Report No. FERMILAB-PUB-82-059-THY (unpublished).
- [11] D. A. Appel, Phys.Rev. **D33**, 717 (1986).
- [12] J. P. Blaizot and L. D. McLerran, Phys.Rev. **D34**, 2739 (1986).
- [13] M. Rammerstorfer and U. W. Heinz, Phys.Rev. **D41**, 306 (1990).
- [14] M. Gyulassy and M. Plumer, Phys.Lett. **B243**, 432 (1990).
- [15] M. H. Thoma and M. Gyulassy, Nucl.Phys. **B351**, 491 (1991).
- [16] M. Gyulassy and X.-N. Wang, Nucl.Phys. **B420**, 583 (1994), arXiv:nucl-th/9306003 [nucl-th].
- [17] G. Aad *et al.* (ATLAS Collaboration), Phys. Rev. Lett. **114**, 072302 (2015), arXiv:1411.2357 [hep-ex].
- [18] J. Adam *et al.* (ALICE Collaboration), Phys. Lett. **B746**, 1 (2015), arXiv:1502.01689 [nucl-ex].
- [19] S. Chatrchyan *et al.* (CMS Collaboration), Report No. CMS-PAS-HIN-12-004 (2012).
- [20] G. Aad *et al.* (ATLAS Collaboration), Phys.Rev.Lett. **105**, 252303 (2010), arXiv:1011.6182 [hep-ex].
- [21] S. Chatrchyan *et al.* (CMS Collaboration), Phys.Rev. **C84**, 024906 (2011), arXiv:1102.1957 [nucl-ex].
- [22] S. Chatrchyan *et al.* (CMS Collaboration), Phys.Lett. **B712**, 176 (2012), arXiv:1202.5022 [nucl-ex].
- [23] S. Chatrchyan *et al.* (CMS Collaboration), JHEP **1210**, 087 (2012), arXiv:1205.5872 [nucl-ex].
- [24] S. Chatrchyan *et al.* (CMS Collaboration), Phys. Lett. **B718**, 773 (2013), arXiv:1205.0206 [nucl-ex].
- [25] G. Aad *et al.* (ATLAS Collaboration), Phys. Lett. **B719**, 220 (2013), arXiv:1208.1967 [hep-ex].
- [26] G. Aad *et al.* (ATLAS Collaboration), Phys. Rev. Lett. **111**, 152301 (2013), arXiv:1306.6469 [hep-ex].
- [27] S. Chatrchyan *et al.* (CMS Collaboration), Phys. Lett. **B730**, 243 (2014), arXiv:1310.0878 [nucl-ex].
- [28] S. Chatrchyan *et al.* (CMS Collaboration), Phys. Rev. **C90**, 024908 (2014), arXiv:1406.0932 [nucl-ex].
- [29] G. Aad *et al.* (ATLAS Collaboration), Phys. Lett. **B739**, 320 (2014), arXiv:1406.2979 [hep-ex].
- [30] G. Aad *et al.* (ATLAS Collaboration), Phys. Lett. **B751**, 376 (2015), arXiv:1506.08656 [hep-ex].
- [31] V. Khachatryan *et al.* (CMS Collaboration), JHEP **01**, 006 (2016), arXiv:1509.09029 [nucl-ex].
- [32] V. Khachatryan *et al.* (CMS Collaboration), JHEP **02**, 156 (2016), arXiv:1601.00079 [nucl-ex].
- [33] I. Vitev and B.-W. Zhang, Phys. Rev. Lett. **104**, 132001 (2010), arXiv:0910.1090 [hep-ph].
- [34] G.-Y. Qin and B. Muller, Phys.Rev.Lett. **106**, 162302 (2011), arXiv:1012.5280 [hep-ph].
- [35] J. Casalderrey-Solana, J. G. Milhano, and U. A. Wiedemann, J.Phys. **G38**, 035006 (2011), arXiv:1012.0745 [hep-ph].
- [36] C. Young, B. Schenke, S. Jeon, and C. Gale, Phys.Rev. **C84**, 024907 (2011), arXiv:1103.5769 [nucl-th].
- [37] Y. He, I. Vitev, and B.-W. Zhang, Phys.Lett. **B713**, 224 (2012), arXiv:1105.2566 [hep-ph].
- [38] T. Renk, Phys.Rev. **C85**, 064908 (2012), arXiv:1202.4579 [hep-ph].
- [39] G.-L. Ma, Phys. Rev. **C87**, 064901 (2013), arXiv:1304.2841 [nucl-th].
- [40] F. Senzel, O. Fochler, J. Uphoff, Z. Xu, and C. Greiner, J. Phys. **G42**, 115104 (2015), arXiv:1309.1657 [hep-ph].
- [41] Y.-T. Chien and I. Vitev, (2015), arXiv:1509.07257 [hep-ph].
- [42] W. Dai, I. Vitev, and B.-W. Zhang, Phys. Rev. Lett. **110**, 142001 (2013), arXiv:1207.5177 [hep-ph].
- [43] X.-N. Wang and Y. Zhu, Phys.Rev.Lett. **111**, 062301 (2013), arXiv:1302.5874 [hep-ph].
- [44] G.-Y. Qin, Eur. Phys. J. **C74**, 2959 (2014), arXiv:1210.6610 [hep-ph].
- [45] Y. Mehtar-Tani, C. A. Salgado, and K. Tywoniuk, Phys. Lett. **B707**, 156 (2012), arXiv:1102.4317 [hep-ph].
- [46] J. Casalderrey-Solana, Y. Mehtar-Tani, C. A. Salgado, and K. Tywoniuk, Phys. Lett. **B725**, 357 (2013), arXiv:1210.7765 [hep-ph].
- [47] J.-P. Blaizot, E. Iancu, and Y. Mehtar-Tani, Phys. Rev. Lett. **111**, 052001 (2013), arXiv:1301.6102 [hep-ph].
- [48] L. Fister and E. Iancu, JHEP **03**, 082 (2015), arXiv:1409.2010 [hep-ph].
- [49] L. Apolinario, N. Armesto, and L. Cunqueiro, JHEP **02**, 022 (2013), arXiv:1211.1161 [hep-ph].
- [50] K. C. Zapp, F. Krauss, and U. A. Wiedemann, JHEP **1303**, 080 (2013), arXiv:1212.1599 [hep-ph].
- [51] A. Majumder, Phys. Rev. **C88**, 014909 (2013), arXiv:1301.5323 [nucl-th].
- [52] J. Casalderrey-Solana, D. C. Gulhan, J. G. Milhano, D. Pablos, and K. Rajagopal, JHEP **10**, 19 (2014), [Erratum: JHEP09,175(2015)], arXiv:1405.3864 [hep-ph].
- [53] J.-P. Blaizot, Y. Mehtar-Tani, and M. A. C. Torres, Phys. Rev. Lett. **114**, 222002 (2015), arXiv:1407.0326 [hep-ph].
- [54] J. Adams *et al.* (STAR Collaboration), Phys. Rev. Lett. **95**, 152301 (2005), arXiv:nucl-ex/0501016 [nucl-ex].
- [55] S. S. Adler *et al.* (PHENIX Collaboration), Phys. Rev. Lett. **97**, 052301 (2006), arXiv:nucl-ex/0507004 [nucl-ex].
- [56] A. Adare *et al.* (PHENIX Collaboration), Phys. Rev. **C78**, 014901 (2008), arXiv:0801.4545 [nucl-ex].
- [57] B. I. Abelev *et al.* (STAR Collaboration), Phys. Rev. Lett. **102**, 052302 (2009), arXiv:0805.0622 [nucl-ex].
- [58] H. Stoecker, Nucl.Phys. **A750**, 121 (2005), arXiv:nucl-th/0406018 [nucl-th].
- [59] J. Casalderrey-Solana, E. V. Shuryak, and D. Teaney, J.Phys.Conf.Ser. **27**, 22 (2005), arXiv:hep-ph/0411315 [hep-ph].
- [60] J. Ruppert and B. Muller, Phys. Lett. **B618**, 123 (2005), arXiv:hep-ph/0503158 [hep-ph].
- [61] L. M. Satarov, H. Stoecker, and I. N. Mishustin, Phys.Lett. **B627**, 64 (2005), arXiv:hep-ph/0505245 [hep-ph].
- [62] T. Renk and J. Ruppert, Phys. Rev. **C73**, 011901 (2006), arXiv:hep-ph/0509036 [hep-ph].
- [63] G. L. Ma *et al.*, Phys. Lett. **B641**, 362 (2006), arXiv:nucl-th/0601012 [nucl-th].
- [64] A. K. Chaudhuri, Phys. Rev. **C75**, 057902 (2007), arXiv:nucl-th/0610121 [nucl-th].
- [65] S. Zhang *et al.*, Phys. Rev. **C76**, 014904 (2007), arXiv:0706.3820 [nucl-th].
- [66] A. K. Chaudhuri, Phys. Rev. **C77**, 027901 (2008), arXiv:0706.3958 [nucl-th].
- [67] W. Li, S. Zhang, Y. G. Ma, X. Z. Cai, J. H. Chen, H. Z. Huang, G. L. Ma, and C. Zhong, Phys. Rev. **C80**, 064913 (2009).
- [68] B. Betz, J. Noronha, G. Torrieri, M. Gyulassy, and D. H. Rischke, Phys.Rev.Lett. **105**, 222301 (2010), arXiv:1005.5461 [nucl-th].
- [69] G.-L. Ma and X.-N. Wang, Phys. Rev. Lett. **106**, 162301 (2011), arXiv:1011.5249 [nucl-th].
- [70] J. Takahashi, B. M. Tavares, W. L. Qian, R. Andrade,

- F. Grassi, Y. Hama, T. Kodama, and N. Xu, Phys. Rev. Lett. **103**, 242301 (2009), arXiv:0902.4870 [nucl-th].
- [71] B. Alver and G. Roland, Phys. Rev. **C81**, 054905 (2010), [Erratum: Phys. Rev. **C82**, 039903(2010)], arXiv:1003.0194 [nucl-th].
- [72] K. Aamodt *et al.* (ALICE Collaboration), Phys. Rev. Lett. **107**, 032301 (2011), arXiv:1105.3865 [nucl-ex].
- [73] Y. Tachibana and T. Hirano, Phys. Rev. **C90**, 021902 (2014), arXiv:1402.6469 [nucl-th].
- [74] Y. He, T. Luo, X.-N. Wang, and Y. Zhu, Phys. Rev. **C91**, 054908 (2015), arXiv:1503.03313 [nucl-th].
- [75] H. Li, F. Liu, G.-l. Ma, X.-N. Wang, and Y. Zhu, Phys. Rev. Lett. **106**, 012301 (2011), arXiv:1006.2893 [nucl-th].
- [76] I. Bouras, B. Betz, Z. Xu, and C. Greiner, Phys. Rev. **C90**, 024904 (2014), arXiv:1401.3019 [hep-ph].
- [77] S. Borsanyi, Z. Fodor, C. Hoelbling, S. D. Katz, S. Krieg, and K. K. Szabo, Phys. Lett. **B730**, 155 (2014), arXiv:1312.2193 [hep-lat].
- [78] T. Hirano and Y. Nara, PTEP **2012**, 01A203 (2012), arXiv:1203.4418 [nucl-th].
- [79] K. Aamodt *et al.* (ALICE Collaboration), Phys. Rev. Lett. **106**, 032301 (2011), arXiv:1012.1657 [nucl-ex].
- [80] J. D. Bjorken, Phys. Rev. **D27**, 140 (1983).
- [81] T. Hirano, P. Huovinen, and Y. Nara, Phys. Rev. **C84**, 011901 (2011), arXiv:1012.3955 [nucl-th].
- [82] F. Cooper and G. Frye, Phys. Rev. **D10**, 186 (1974).
- [83] R. B. Neufeld and B. Muller, Phys. Rev. Lett. **103**, 042301 (2009), arXiv:0902.2950 [nucl-th].
- [84] G.-Y. Qin, A. Majumder, H. Song, and U. Heinz, Phys. Rev. Lett. **103**, 152303 (2009), arXiv:0903.2255 [nucl-th].
- [85] R. B. Neufeld and I. Vitev, Phys. Rev. **C86**, 024905 (2012), arXiv:1105.2067 [hep-ph].
- [86] R. B. Neufeld, Phys. Rev. **C79**, 054909 (2009), arXiv:0807.2996 [nucl-th].
- [87] R. B. Neufeld and T. Renk, Phys. Rev. **C82**, 044903 (2010), arXiv:1001.5068 [nucl-th].
- [88] I. Bouras, A. El, O. Fochler, H. Niemi, Z. Xu, *et al.*, Phys. Lett. **B710**, 641 (2012), arXiv:1201.5005 [nucl-th].
- [89] A. Dainese, C. Loizides, and G. Paic, Eur. Phys. J. **C38**, 461 (2005), arXiv:hep-ph/0406201 [hep-ph].
- [90] T. Renk, Phys. Rev. **C74**, 024903 (2006), arXiv:hep-ph/0602045 [hep-ph].
- [91] T. Renk and K. J. Eskola, Phys. Rev. **C75**, 054910 (2007), arXiv:hep-ph/0610059 [hep-ph].